ASCE

Experimental Investigation and Modeling of the Thermal Effect on the Mechanical Properties of Polyethylene-Terephthalate FRP Laminates

Haya H. Mhanna[1]; Rami A. Hawileh, Ph.D., M.ASCE[2]; Wael Abuzaid, Ph.D.[3]; M. Z. Naser, Ph.D., M.ASCE[4]; and Jamal A. Abdalla, Ph.D., F.ASCE[5]

Abstract: Recent advancements in material sciences have led to the development of new fiber-reinforced polymer (FRP) systems that, unlike traditional FRPs, are specifically tailored to have large fracture strains that are advantageous for external strengthening applications. One such system is polyethylene terephthalate (PET) FRP, which can attain a nominal fracture strain of 7%. In this work, the mechanical properties of PET laminates were investigated when exposed to temperatures ranging from 25°C to 125°C. Test results indicate that PET-FRP exhibits a nonlinear stress-strain response that could be divided into three phases with three moduli (E_1, E_2, and E_3) and corresponding three tensile strengths (σ_1, σ_2, and σ_3). The results also demonstrate how the aforementioned mechanical properties degrade around the glass transition temperature of the epoxy from so ft ening in the matrix. Interestingly, test results indicate that PETs exhibit an increase in rupture strain (from 9% to 14%) when the test temperature increases from 25°C to 125°C. To properly document these observations into design tools, temperature-dependent material models for moduli and tensile strengths are derived. **DOI: 10.1061/(ASCE)MT.1943-5533.0003389.**

Author keywords: Fiber-reinforced polymers (FRP); Polyethylene terephthalate (PET); Large rupture strain (LRS); External strengthening; Digital image correlation (DIC).

Introduction

The interest in applying fiber-reinforced polymer (FRP) materials to reinforced concrete (RC) structures to retrofit applications has increased over the last few decades (Hawileh et al. 2014). FRP materials exhibit superior properties, such as high strength-to-weight ratios, corrosion resistance, and desirable characteristics (e.g., ease of installment and versatility). External strengthening using FRP materials enhances the axial, flexural, and shear capacity of structural RC members, and improves their ductility and durability performance (Hawileh and Naser 2012; Hawileh et al. 2014, 2015b; Ou and Zhu 2015).

The conventional FRP types used in the retrofitting industry are carbon-FRP (CFRP), glass-FRP (GFRP), and Aaramid-FRP (AFRP). These FRP composites have a linear elastic behavior and fail in a brittle manner at very low strains (typically in the range of 1.5%–3%). As such, commonly used FRP strengthening systems are never utilized to their full-strength capacity (Dai et al. 2011; Saleem et al. 2017). Despite this limitation, numerous studies have indicated that conventional FRP laminates can be successfully used to confine structural elements in seismic applications, thus increasing their axial and shear strengths. However, the tendency of fibers to fracture at low strain levels impairs confinement and leads to a sudden and catastrophic failure. Hence, new FRP materials with large rupture strains (LRS) have emerged as alternatives to conventional FRP materials. Commercially available LRS-FRPs are manufactured from recycled polymers, namely, polyethylene naphthalate (PEN), polyethylene terephthalate (PET), and polyacetal fiber (PAF) (Anggawidjaja et al. 2006; Dai et al. 2012). The stress-strain behavior of conventional FRPs (e.g., CFRP and GFRP) and LRS-FRPs is provided in Fig. 1. Compared with their conventional counterparts, LRP-FRPs have improved rupture strains (approximately 20%–40% higher). The strength levels, although inferior relative to CFRP and other conventional FRPs, are still comparable to steel. The use of steel in external strengthening applications is curtailed by its poor corrosion resistance. In addition, noted is that high-strength and brittle FRP is never completely utilized to its full-strength capacity in external strengthening applications (Ali et al. 2014; Shekarchi et al. 2018). In addition to their desirable mechanical properties, LRS-FRPs have the additional advantage of being more economical and environmentally friendly than conventional FRPs (Borg et al. 2016).

Recent efforts focused on the use of LRS-FRPs for external strengthening and confining applications (i.e., full external wrapping) at ambient deformation conditions (Huang et al. 2018; Pimanmas and Saleem 2018). These studies provided experimental

[1]Graduate Student, Dept. of Civil Engineering, American Univ. of Sharjah, P.O. Box 26666, Sharjah, United Arab Emirates. Email: g00023682@alumni.aus.edu

[2]Professor, Dept. of Civil Engineering, American Univ. of Sharjah, P.O. Box 26666, Sharjah, United Arab Emirates (corresponding author). Email: rhaweeleh@aus.edu

[3]Assistant Professor, Dept. of Mechanical Engineering, American Univ. of Sharjah, P.O. Box 26666, Sharjah, United Arab Emirates. Email: wabuzaid@aus.edu

[4]Assistant Professor, Glenn Dept. of Civil Engineering, Clemson Univ., 312 Lowry Hall, Clemson, SC 29634. ORCID: https://orcid.org/0000-0003-1350-3654. Email: mznaser@clemson.edu

[5]Professor, Dept. of Civil Engineering, American Univ. of Sharjah, P.O. Box 26666, Sharjah, United Arab Emirates. Email: jabdalla@aus.edu

Note. This manuscript was submitted on December 30, 2019; approved on April 7, 2020; published online on July 29, 2020. Discussion period open until December 29, 2020; separate discussions must be submitted for individual papers. This paper is part of the ***Journal of Materials in Civil Engineering***, © ASCE, ISSN 0899-1561.

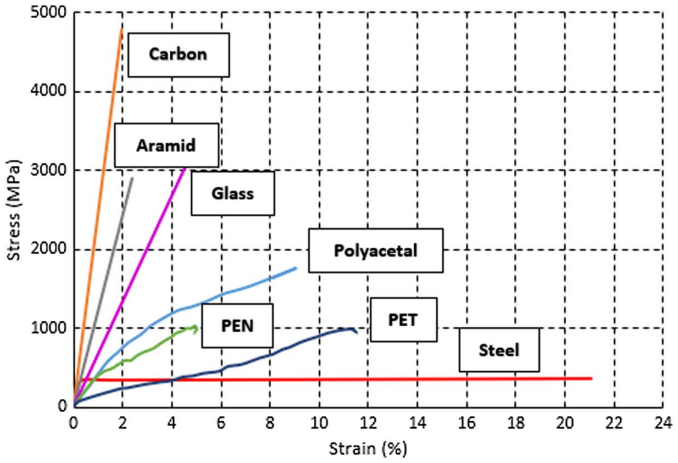

Fig. 1. Stress-strain curves for several types of FRP and steel. [Reprinted from *Cement and Concrete Composites*, Vol. 28 (10), D. Anggawidjaja, T. Ueda, J. Dai, and H. Nakai, "Deformation capacity of RC piers wrapped by new fiber-reinforced polymer with large fracture strain," pp. 914–927, © 2006, with permission from Elsevier.]

evidence that PETs can be a suitable option for confining columns for seismic retrofitting purposes. Some studies (Anggawidjaja et al. 2006; Zhang et al. 2017) also verified that PET fibers increase the shear capacity of shear deficient columns if sufficient layers of PET-FRP sheets are provided. Thus, the large ductility of PET-FRP materials brings in new opportunities to better fine-tune traditional FRP systems and presents solutions to extraordinary problems, such as poor ductility and premature debonding of FRP-strengthened systems. For example, PET-FRP systems can be used in a hybrid combination with CFRP laminates to allow modern FRP strengthening systems to achieve much-improved ductile performance. This ductile performance can be advantageous under a variety of loading conditions, such as static, cyclic, and impact.

Because retrofitting applications often integrate FRP systems into the external face of weakened structures, FRPs are usually exposed to open and potentially harsh environments (Al-Tamimi et al. 2015; El-Dieb et al. 2012; El-Hassan and El Maaddawy 2019). Temperature exposure is of particular interest because the utilized polymeric materials generally exhibit strong temperature dependence through their mechanical properties with limited temperature increases (approximately 25°C–75°C) (Hawileh et al. 2009, 2015a) and significant so ft ening beyond their glass transition temperature (T_g) (60°C–110°C) (Ou et al. 2016; Reis et al. 2012). Whereas a number of studies investigated the mechanical properties of conventional FRP materials under elevated temperatures (Chowdhury et al. 2011; Correia et al. 2013; Wang et al. 2011; Zhou et al. 2019), other studies that aimed to investigate the properties of new LRS-FRP materials, such as PET, PEN, and PAF, under elevated temperatures remain limited. A proper understanding of the temperature-dependent mechanical properties of these reinforcement systems is crucial to designing and analyzing external strengthened RC members exposed to high temperature environments.

The main goal of this paper is to investigate the mechanical properties of PET-FRP laminates at temperatures ranging from 25°C–125°C, both experimentally and analytically. Full-field and noncontact strain measurements were collected using the digital image correlation (DIC) technique to provide an accurate and reliable assessment of deformation at the considered temperature range. Overall, the work provides quantitative insights into the temperature-dependent mechanical properties (i.e., stress-strain response, stiffness, Poisson's ratio, ductility, strength, and damage) of PET-FRP laminates. In addition, temperature-dependent material models are proposed to predict the moduli and strengths for temperatures ranging from 25°C to 125°C, which will aid in the development of external strengthening systems on the basis of this LRS-FRP material.

Table 1. Mechanical properties of FRP sheets and epoxy adhesive at room temperature

Material	Elastic modulus (GPa)	Tensile strength (MPa)	Elongation at rupture (%)	Sheet thickness (mm)
PET-600	10 ± 1	740	≥7	0.841
Epoxy adhesive (MapeWrap 31SP)	1	28	3.4	—

Experimental Program

Material Properties

In this study, PET-600 fiber reinforcement material along with MapeWrap 31SP, a two-component medium-viscosity epoxy adhesive, were used to manufacture PET-LRS laminates. The mechanical properties reported by manufacturers of the PET fibers and cured epoxy polymer (glass transition temperature $T_g > 70$°C) are listed in Table 1.

Sample Preparation

A total of 15 specimens were prepared and tested to investigate the mechanical properties of the PET-FRP laminates at temperatures ranging from 25°C to 125°C. Three specimens were investigated at each deformation temperature. Specimens were prepared and tested according to provisions of the ASTM D3039/D3039 M guidelines (ASTM 2008). The two-part epoxy material was mixed using a 3:1 weight ratio as recommended by the manufacturer. Single-layer PET-FRP sheets were produced using standard wet layup techniques. The epoxy-impregnated PET sheets were cured in a compression molding machine for 2 h at 80°C, and then were kept at room temperature for 7 days prior to testing. Coupon specimens were cut using a laser cutting machine. The width and total length of each coupon specimen were 15 and 200 mm, respectively. Rectangular pieces made of flame-retardant Garolite were glued to both sides of the gripping section to prevent premature failure at the specimen-grips interface. A speckle pattern for DIC measurements was applied to the gauge section using a high temperature paint (rated for temperatures up to 200°C). A schematic and a picture of one of the prepared specimens and a paint pattern are provided in Fig. 2. The subset size used for DIC correlations is indicated with a box in the zoomed optical image in Fig. 2.

Test Procedure

All specimens were loaded using a screw-driven Instron (Norwood, Massachusetts) machine equipped with an environmental chamber. Deformation was applied in displacement control at a rate of 1 mm/min to failure, following a 30-min soaking time at the desired deformation temperature. The soaking time assures a homogeneous temperature in the entire specimen prior to load application. During deformation, optical images of the sample's surface were captured every 2 s to allow for full-field strain measurements. All correlations were conducted using commercial DIC so ft ware (Vic-2D version 2009 from Correlated Solutions). The global strains were calculated by averaging the DIC strain fields

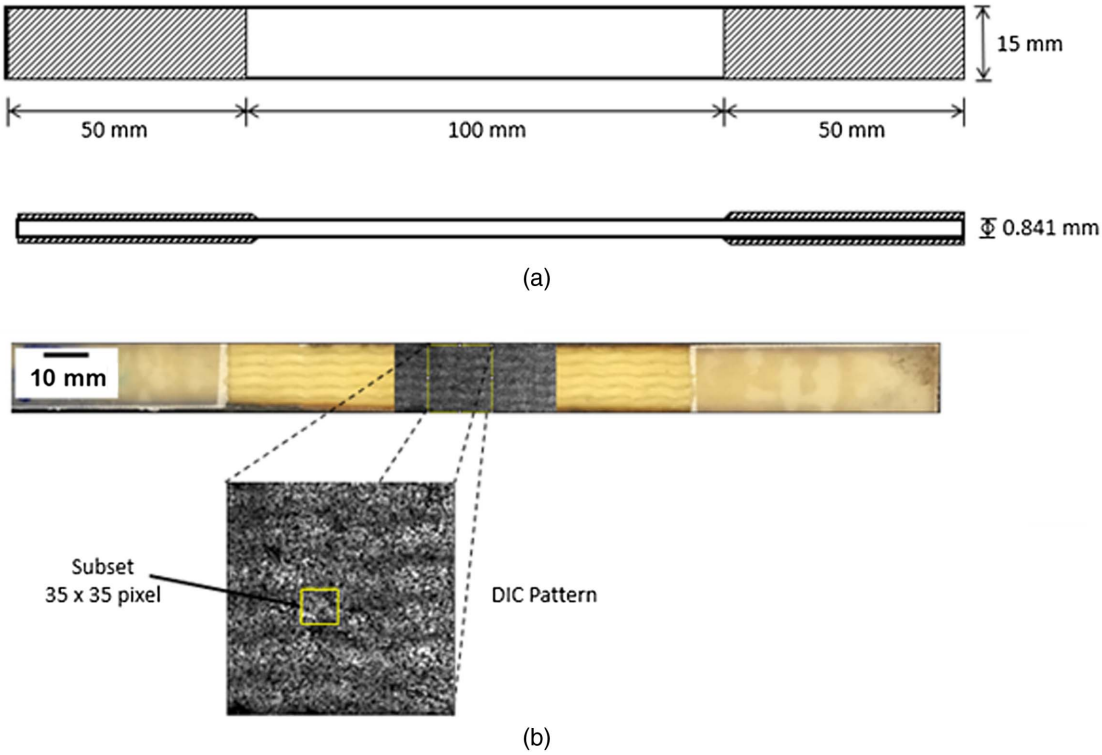

Fig. 2. (a) Schematic of each specimen; and (b) actual specimen. A high temperature speckle pattern was added to the gauge section for DIC measurements. The subset size used for DIC correlations is indicated with a box in the zoomed optical image.

along the loading direction in a 20 × 11 mm gauge section on the sample's surface (i.e., the correlation window defined on the sample's surface).

Results and Discussion

As explained previously, this work focuses on evaluating the temperature-dependent mechanical properties (tensile strength, Poisson's ratio, and modulus) of PET-600 laminates. Fig. 3 indicates the representative stress-strain curves of specimens loaded at various deformation temperatures.

All of the stress-strain curves reported in Fig. 3 exhibit a nonlinear response associated with viscoelastic and plastic behavior of this composite material. This observation is consistent with previous results reported for PET-FRP composites (Dai et al. 2011; Pimanmas and Saleem 2018; Saleem et al. 2017, 2018). In those studies, the room temperature behavior was divided into two phases with two moduli, E_1 and E_2. However, the results reported in this work at higher deformation temperatures point to a more complicated response. Initially, the modulus in all tested samples is high, and then its magnitude starts to decrease, followed by a gradual increase before the sample fractures. The physical representation of the three phases was laid out by Lechat et al. (2011). In this particular study, Lechat et al. (2011) noted how the initial increase in the modulus arises from disentanglement of the carbon chains. Following this phase, the fast drop in the modulus is due to a restructuring of the amorphous phase. Aft er that, the modulus undergoes another progressive increase as the molecular backbone is being loaded. Finally, the modulus decreases due to failure.

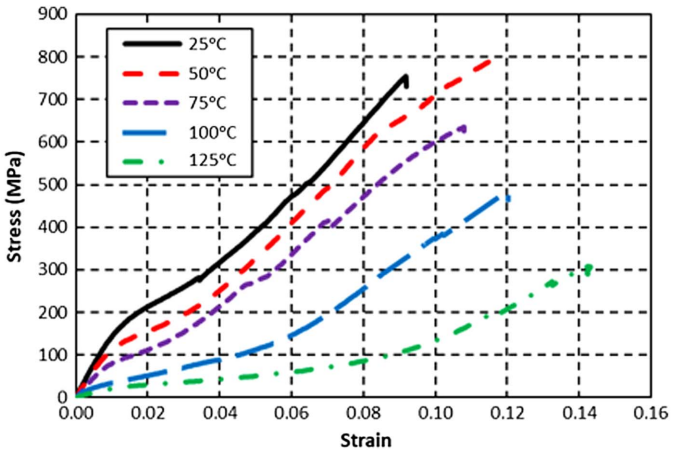

Fig. 3. Stress-strain responses of PET FRP as a function of temperature.

All samples shared approximately the same strain (0.5%) at which the first change in stiffness was observed. However, the strains at which the second change in stiffness occurs is temperature dependent and ranges from 1.5% to 8%. To provide insights into the material's nonlinearity, a specimen was subjected to multiple loading and unloading cycles, as indicated in Fig. 4. In the first cycles, the sample was loaded up to approximately 100 MPa, which was lower than the stress/strain levels at which stiffness reduction was observed for room temperature deformation. The complete recovery on unloading is indicative of pure elastic behavior. In the second cycle, the sample was deformed beyond the point of stiffness change and reached a stress of approximately 235 MPa. On unloading, and despite large levels of strain recovery, a finite residual plastic strain was measured (0.0028 mm/mm, as indicated by point B in Fig. 4). In the third loading cycle, more pronounced levels of plastic strain (0.0242 mm/mm, indicated by point C in Fig. 4) were measured along with an additional transition (i.e., increase) in stiffness levels. Based on the observations and measurements of residual

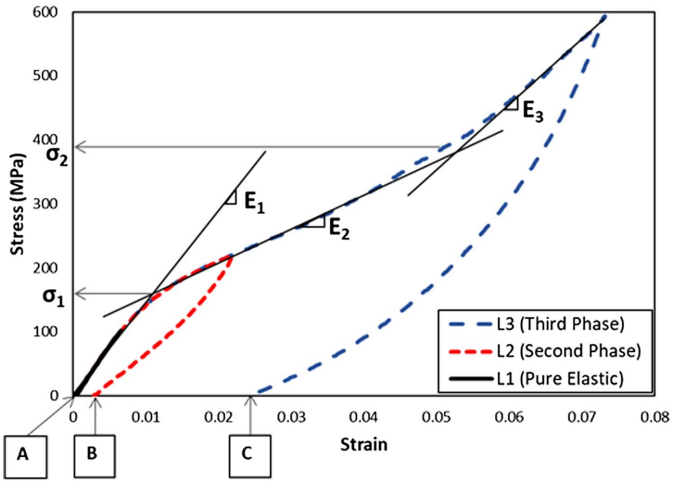

Fig. 4. Loading and unloading cycles for a laminate PET at room temperature with the demonstration of obtaining the three moduli (E_1, E_2, and E_3) and tensile strengths (σ_1 and σ_2).

plastic strains indicated in Fig. 4, the first slope (elastic loading L1) is considered the elastic modulus and is referred to as E_1. The other two moduli are referred to as E_2 (first stiffness change) and E_3 (second stiffness change), corresponding to the slopes of the second and third phases, respectively. The three moduli are clearly marked in Fig. 4, along with the stress levels, σ_1 and σ_2, which identify the onset of the transition between the three stages as defined using the stiffness magnitude. The third stress (σ_3), which is not provided in Fig. 4, represents the ultimate tensile strength at fracture.

Table 2 summarizes the average results of the elastic modulus E_1, moduli (E_2 and E_3), average rupture strain (ε_{rup}), and tensile strengths (σ_1, σ_2, and σ_3), along with their relative standard deviation (RSD) at all considered temperature levels. The range of RSD for all of the properties is between 0.17% and 16.72%. Values of the average normalized moduli (E_1/E_{25}), (E_2/E_{25}), and (E_3/E_{25}) and the average normalized tensile strength (σ_1/σ_{25}), (σ_2/σ_{25}), and (σ_3/σ_{25}) at each temperature are presented in Table 3, where E_{25} and σ_{25} are the moduli (E_1, E_2, and E_3) and tensile strengths (σ_1, σ_2, and σ_3) at room temperature, respectively. In addition, the degradation of the normalized moduli and average tensile strengths of the PET laminates as a function of increasing temperature is provided in Fig. 5. Moreover, Table 4 presents the maximum measured degradation in properties, moduli (E_1, E_2, and E_3), and tensile strengths (σ_1, σ_2, and σ_3), which occurred at 125°C deformation temperature. Although all reported measurements point to a significant degradation in mechanical properties, the effects were more pronounced in the first (i.e., first stiffness change) and second stages of deformation.

Table 3. Normalized moduli and tensile strengths of PET-FRP laminates at tested temperatures

Temperature	E_1/E_{25}	E_2/E_{25}	E_3/E_{25}	σ_1/σ_{25}	σ_2/σ_{25}	σ_3/σ_{25}
25	1.00	1.00	1.00	1.00	1.00	1.00
50	0.82	0.72	0.79	0.80	0.49	1.00
75	0.64	0.56	0.75	0.62	0.36	0.78
100	0.29	0.30	0.64	0.29	0.29	0.62
125	0.15	0.14	0.45	0.14	0.23	0.40

In general, the results presented in Figs. 3 and 5 and Tables 2–4 point to a clear reduction in strength and stiffness with an increase in deformation temperature. However, specimens deformed at 50°C deviated from the aforementioned trend and exhibited an enhancement in strength and rupture strain relative to specimens deformed at room temperature. For example, σ_3 increased from 736 MPa at a 25°C deformation temperature to 766 MPa at 50°C. The rupture strain ε_{rup} increased from 0.0903 to 0.1141 mm/mm in the same temperature range. This increase could be related to the phenomenon associated with the additional curing effects of epoxy adhesive within the laminate induced by heat exposure at a temperature lower than T_g. Typically, the mechanical properties of the epoxy are enhanced at higher temperatures lower than T_g due to increased production of cross-links that, in turn, provides enough kinetic energy to quickly initiate chemical reactions at even the most hindered locations (Benedetti et al. 2015). Thus, such an improvement in the mechanical properties of the epoxy enhances the tensile strength of the laminates, which is pronounced in the enhancement of tensile strength of the PET-FRP laminates at 50°C. At 75°C, that is, higher than the glass transition temperature of the epoxy, the ultimate tensile strength starts degrading and reaches a value of 305 MPa at 125°C due to so ft ening of the resin matrix. However, ε_{rup} increases with increasing temperatures and reaches a value of 0.1419 mm/mm (14.19%) at 125°C. According to Table 4, E_1 and E_2 degrade by 85% at 125°C, whereas E_3 degrades by 54%. Similarly, σ_1 and σ_2 degrade by 85.77% and 77.50%, respectively, whereas σ_3 degrades by 60% at 125°C. These results indicate that an increasing temperature mostly affects the mechanical properties during the first two stages. Also noted from Tables 2 and 3 is that, at 100°C, PET-FRP experiences more than a 50% loss in its mechanical properties.

In addition to the stiffness strength measures previously reported, the full-field DIC data were used to evaluate the temperature-dependent Poisson's ratio, as indicated in Fig. 6. The Poisson's ratio was determined by plotting lateral strain (ε_{xx}) against longitudinal strain (ε_{yy}) and then calculating the slope of the initial straight line. The Poisson ratio of PET-FRP is 0.486 at room temperature, as indicated in Fig. 6. This value is considered high relative to other FRP types, such as CFRP, which has a Poisson's ratio in the range of 0.2. The value of Poisson's ratio increases as the temperature increases until it reaches a value of 0.573 at

Table 2. Test results in terms of moduli, rupture strain, and strength

Temperature (°C)	E_1 (GPa)	E_2 (GPa)	E_3 (GPa)	ε_{rup}	σ_1 (MPa)	σ_2 (MPa)	σ_3 (MPa)
25	16.08 ± 0.35	5.48 ± 0.91	9.00 ± 0.99	0.090 ± 0.005	99.1 ± 3.9	317.9 ± 0.6	763.5 ± 112.2
50	13.22 ± 0.30	3.96 ± 0.11	7.11 ± 0.41	0.114 ± 0.002	79.5 ± 2.9	155.1 ± 0.6	766.1 ± 47.5
75	10.22 ± 0.33	3.07 ± 0.19	6.73 ± 0.87	0.098 ± 0.013	61.2 ± 4.2	113.6 ± 6.7	592.6 ± 39.7
100	4.65 ± 0.56	1.63 ± 0.21	5.74 ± 0.28	0.117 ± 0.006	29.0 ± 2.4	91.1 ± 2.1	475.0 ± 18.5
125	2.40 ± 0.12	0.79 ± 0.01	4.08 ± 0.20	0.142 ± 0.002	14.3 ± 0.3	71.5 ± 0.6	305.0 ± 7.6

Note: Ranges based on one standard deviation.

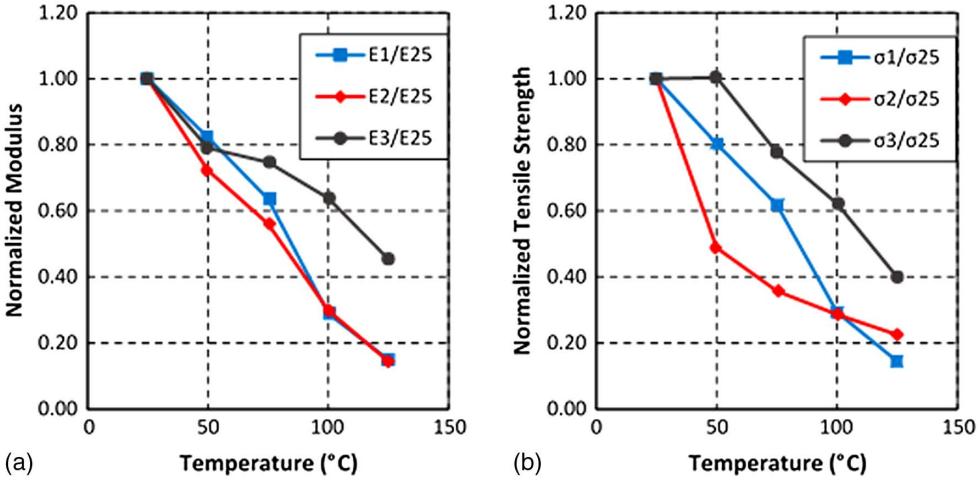

Fig. 5. Degradation of normalized moduli and tensile strengths as a function of temperature: (a) normalized moduli; and (b) normalized tensile strengths.

125°C. Such values would assist in the analysis of strengthened concrete members with such PET-FRP laminates.

Modeling of Mechanical Properties at Elevated Temperature

Comparison of Test Results with Analytical Models

In this section, the experimental results of this study are predicted using existing analytical models in the literature that simulate the degradation of the mechanical properties of FRP materials at elevated temperatures. To be noted is that most of the models present in the literature are based on CFRP and GFRP materials, and the performance of large rupture strain FRP laminates is still lacking information, such as PET under elevated temperatures. Hence, new models based on Gibson et al. (2006) model will be proposed to predict moduli E_1, E_2, and E_3 and tensile strengths σ_1, σ_2, and σ_3 of PET-FRP laminates. An overview of the previous modeling works focusing on CFRP and GFRP laminates is provided in the Appendix.

Table 4. Percent degradation in mechanical properties of PET-FRP laminates at 125°C

Mechanical property	Degradation (%) $= \left(\frac{X_{125} - X_{25}}{X_{25}}\right) \times 100$
E_1	85.06
E_2	85.64
E_3	54.63
σ_1	85.57
σ_2	77.50
σ_3	60.05

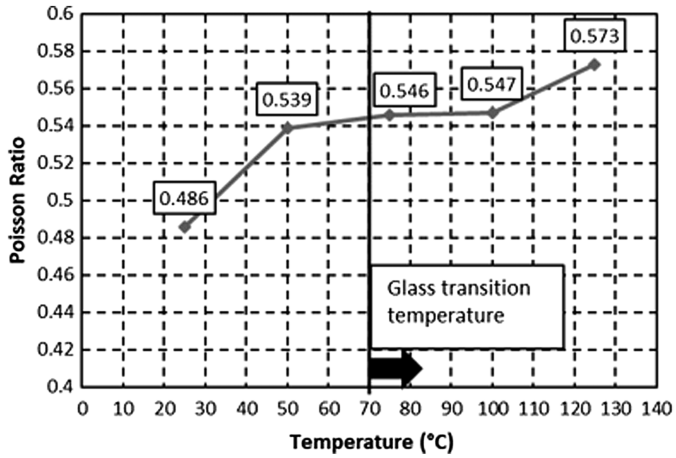

Fig. 6. Poisson ratio as a function of temperature.

Fig. 7 plots the variation in the temperature of the normalized moduli (E_1, E_2, and E_3) and normalized tensile strengths (σ_1, σ_2, and σ_3) of the tested PET-FRP laminates with the predicted results from the different models presented herein. According to Fig. 7, the model proposed by Gu and Asaro (2005), with an m value of 0.5 and the model proposed by Hawileh et al. (2016) for CFRP laminates reasonably estimate the average degradation of the moduli and tensile strengths relative to other models (see the Appendix for model descriptions and utilized equations). The reason for this is that the Gu and Asaro (2005) and Hawileh et al. (2016) models were based on experimental investigations into FRP laminates (not rods or strips) prepared by the wet layup technique, in which fibers are impregnated from sides with epoxy adhesive—similar to this study. In addition, the models proposed by Gu and Asaro (2005) and Hawileh et al. (2016) were based on experimental data from different types of FRP laminates and their hybrid combinations. The differences between the two models arise due to the form of the best-fit equations that predict the mechanical properties of the laminates. For instance, the model proposed by Gu and Asaro (2005) was based on a material degradation model in the form of a power law presented in the variable m in Eq. (7), for which a value of 0 indicates no degradation, and a value of 1 indicates a linear degradation of the mechanical property with temperature. In contrast, the model proposed by Hawileh et al. (2016) was based on a hyperbolic tangent function from Gibson et al. (2006). In addition, CFRP, GFRP, and BFRP laminates and their hybrid combinations have different mechanical properties, such as different tensile strengths, elastic modulus, and rupture strain, and behave in a different manner when exposed to high temperatures.

The other models did not accurately predict the behavior of PET-FRP laminates at elevated temperatures. The reason for the variation between these models and the test results is that most models are based on test results conducted on near surface mounted (NSM) strips and rebars and not laminates prepared by a wet layup

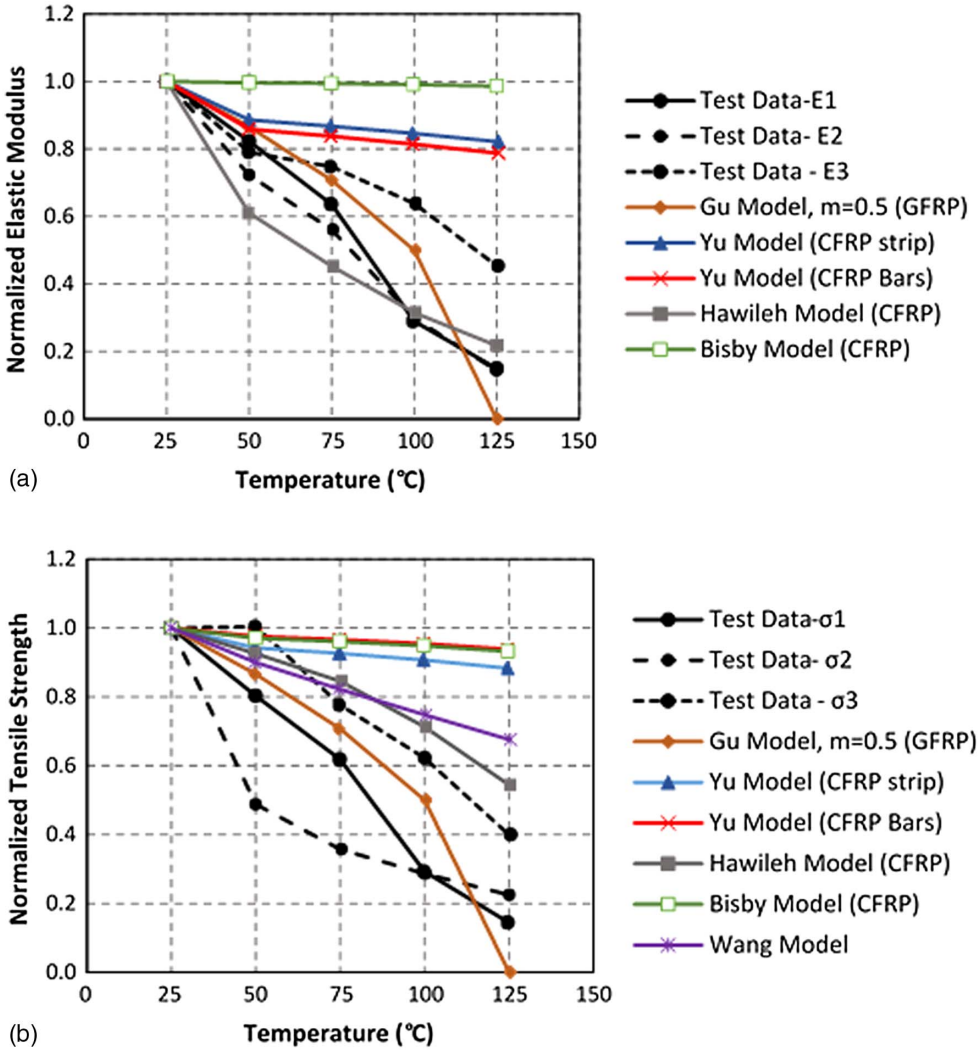

Fig. 7. Comparison between measured test data and predicted results using published models in the literature: (a) normalized moduli (E_1, E_2, and E_3); and (b) normalized tensile strengths (σ_1, σ_2, and σ_3).

Table 5. Derived coefficients for mechanical properties of PET FRP laminates

Coefficient	E_1	E_2	E_3	σ_1	σ_2	σ_3
P_u	1.00	1.00	1.00	1.00	1.00	1.00
P_R	0.15	0.14	0.45	0.14	0.23	0.40
k_m	0.032	0.024	0.018	0.029	0.020	0.034
T'	76.52	69.65	72.43	75.61	33.45	87.46
NSME	0.00133	0.00155	0.00227	0.00128	0.00017	0.00197
MAPE (%)	10.82	12.91	7.75	11.06	3.85	7.05
R	0.99	0.98	0.93	0.99	0.99	0.98

process. In addition, the nonlinear behavior of PET-FRP—as opposed to the linear and brittle behavior of the CFRP and GFRP materials—could contribute to the deviation of the empirical models from the current test results. Hence, new models are proposed in the following section to predict moduli E_1, E_2, and E_3 and tensile strengths σ_1, σ_2, and σ_3 on the basis of the Gibson et al. (2006) model.

Proposed Models

In the current study, a least square regression analysis was used to determine coefficients k_m and T' for normalized moduli E_1, E_2, and E_3 and normalized tensile strengths σ_1, σ_2, and σ_3 using Eq. (8) (Gibson et al. 2006). A Microsoft Excel "solver" function was used to obtain a minimum square error between the measured test data and the empirical model. The mechanical property at 125°C and 25°C was used as P_R and P_u in Eq. (8), respectively. Calculated coefficients based on a regression analysis are provided in Table 5. In addition, the normalized mean square error (NMSE), mean absolute percent error (MAPE), and correlation coefficient (R) for each mechanical property are reported in Table 5.

The following models are proposed using the regression analysis results in Table 5. The developed models presented in Eqs. (1)–(6) predict the normalized moduli E_1, E_2, and E_3 and normalized tensile strengths σ_1, σ_2, and σ_3 of PET-FRP as a function of temperature, respectively

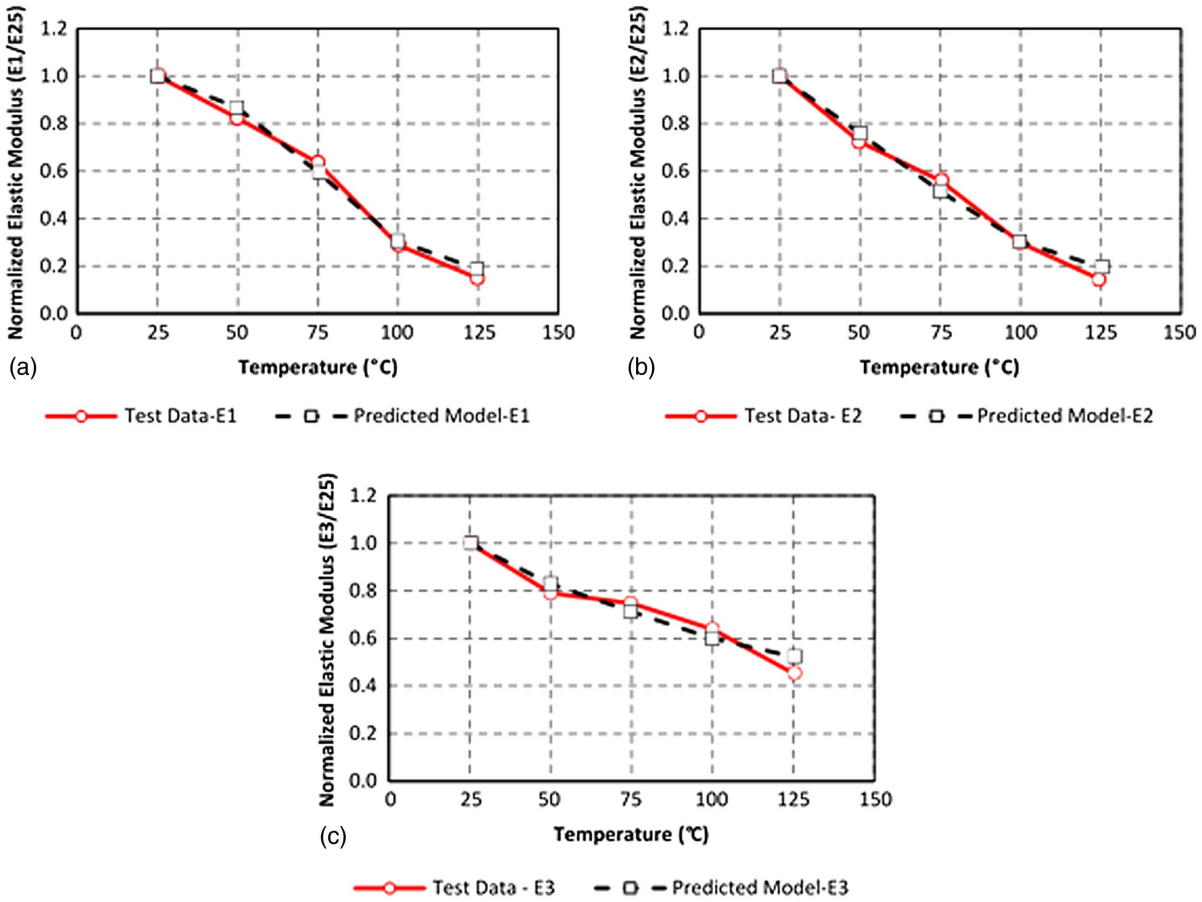

Fig. 8. Comparison between test data and proposed empirical models for E_1, E_2, and E_3: (a) E_1/E_{25}; (b) E_2/E_{25}; and (c) E_3/E_{25}.

$$E_1(T) = 0.575 - 0.425\tanh[0.032(T - 76.52)] \quad (1)$$

$$E_2(T) = 0.572 - 0.428\tanh[0.024(T - 69.65)] \quad (2)$$

$$E_3(T) = 0.727 - 0.273\tanh[0.018(T - 72.43)] \quad (3)$$

$$\sigma_1(T) = 0.572 - 0.429\tanh[0.029(T - 75.61)] \quad (4)$$

$$\sigma_2(T) = 0.613 - 0.387\tanh[0.020(T - 33.45)] \quad (5)$$

$$\sigma_3(T) = 0.700 - 0.300\tanh[0.034(T - 87.46)] \quad (6)$$

Worth noting is that $E_1(T)$ and $\sigma_1(T)$ have very close k_m and T' coefficients, resulting in similar Eqs. (1) and (4). Figs. 8 and 9 provide a comparison between the test results and the proposed empirical models for normalized moduli E_1, E_2, and E_3 and the normalized tensile strengths σ_1, σ_2, and σ_3, respectively. Figs. 8 and 9 indicate that the predicted empirical relations provide reasonable agreement with the measured test data within the temperature range of 25°C–125°C. In addition, Table 5 indicates that the NSME values for all moduli and tensile strengths are small and have a maximum value of 0.00227. Similarly, MAPE values range from 3.85% to 12.91%, with the maximum error occurring at 125°C. Furthermore, all of the R values in Table 5 are to 1.0 for all mechanical parameters indicating a close correlation between the proposed models and the test data. The advantage of applying the proposed models presented in this study, as opposed to the Gu and Asaro (2005) and Hawileh et al. (2016) models, is that the proposed models can reasonably estimate the degradation in the mechanical nonlinear properties of the three phases for the PET-FRP laminates. The models proposed by Gu and Asaro (2005) and Hawileh et al. (2016) were developed for elastic FRP laminates. Thus, such models may not accurately predict the degradation in the mechanics of multiphased FRP materials, such as PETs. Hence, models using experimental investigations into elastic linear composites, such as CFRP, GFRP, and BFRP laminates, cannot be implemented to predict the degradation in the mechanical properties at elevated temperatures of nonlinear composites, such as PET-FRP laminates. As a result, the proposed models are reliable estimates of the degradation of mechanical properties for PET-FRP laminates under elevated temperatures when designing and analyzing externally strengthened concrete members.

Effect of Temperature on Damage Initiation of PET-FRP Laminates

To assess damage initiation of PET-FRP laminates, the material response was investigated on global and local levels. Fig. 10 indicates the stress-strain response of a PET-FRP laminate tested at room temperature along with DIC images representing the longitudinal strain (ε_{yy}) fields at four stress levels denoted by points A, B, C, and D at each loading phase. The two curves indicated in Fig. 10 represent the global response, for which the strain is calculated over a large representative area, and the local response related to strains is extracted from localized regions exhibiting high levels of strain, as indicated in full-field DIC strain maps. DIC images presented in Fig. 10 clearly indicate that the strain distribution along the laminate's length is not uniform. This behavior is associated with the

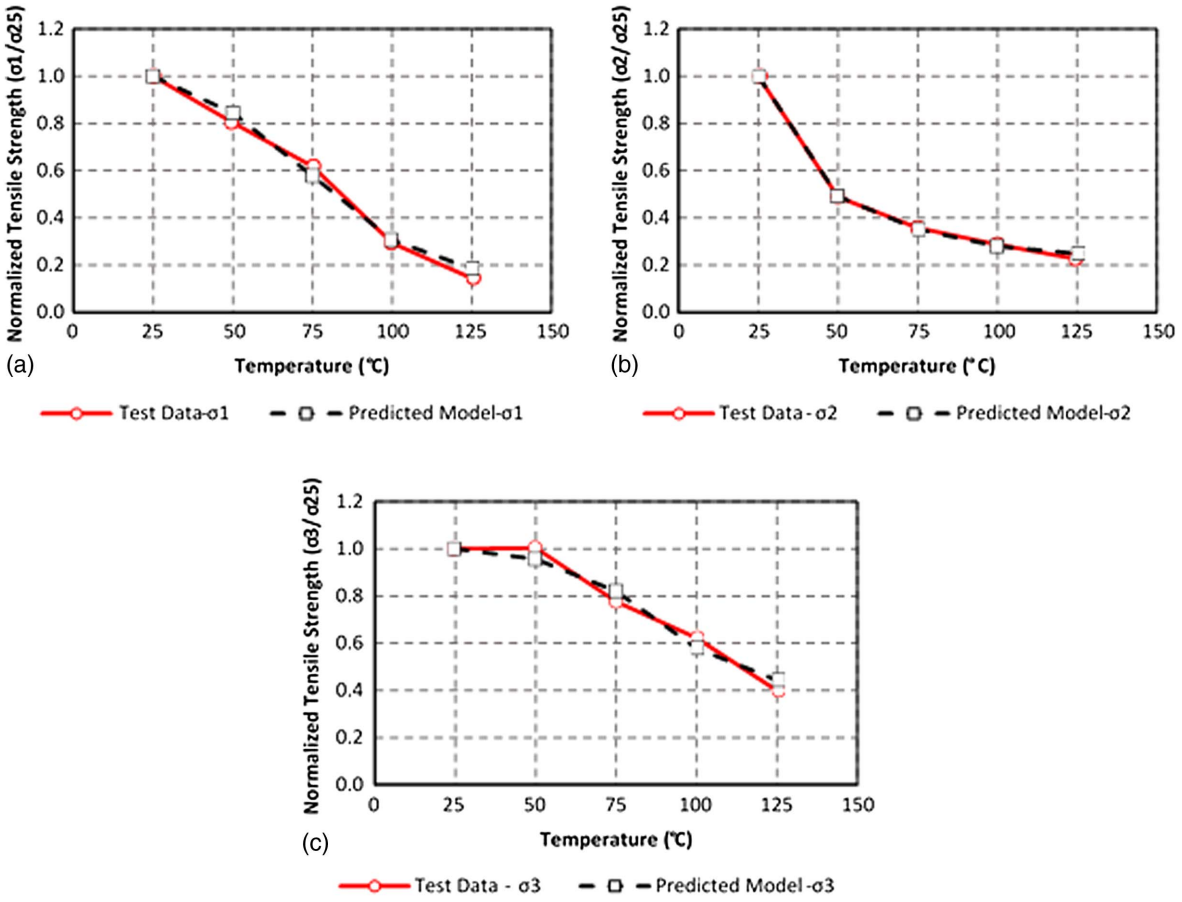

Fig. 9. Comparison between test data and proposed empirical models for σ_1, σ_2, and σ_3: (a) σ_1/σ_{25}; (b) σ_2/σ_{25}; and (c) σ_3/σ_{25}.

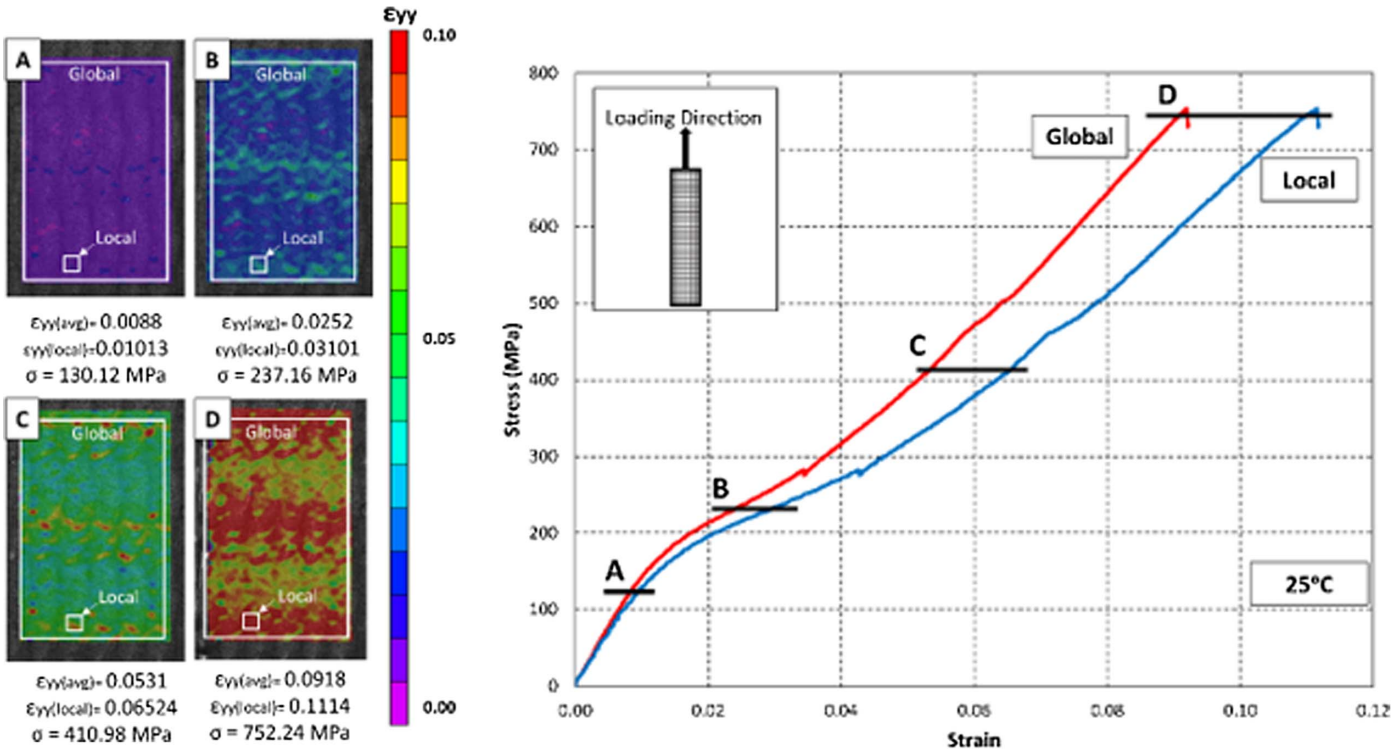

Fig. 10. Stress-strain curves for PET-FRP sample at room temperature indicating variation between local and global strains.

inherent material heterogeneity and the orthotropic characteristics of the laminate. Initially, the stress-strain curves of both local and global responses coincide, indicating no damage in the material. Subsequently, the local curve deviates from the global curve associated with strain localization induced primarily by the initiation of permanent damage in the local area. Important to note is that strain localization is also partially induced by structural heterogeneity and high local stress fields. Therefore, pinpointing the onset of damage on the basis of strain localization measurements requires additional information. In this work, the onset of damage was evaluated using local strain measurements along with observations of damage—defined here as the accumulation of permanent residual strain—from incremental loading and unloading experiments. Fig. 11(a) indicates the stress-strain curves of the loading and unloading cycles. In addition, Fig. 11(b) presents the ratio of local to global strain plotted against the average strain. According to Fig. 11(a), the L1 graph associated with the elastic phase recovers its strain and goes back to its original position on unloading. This behavior can also be noted from Fig. 11(b), in which the ratio of local to global strain in the elastic region remains almost 1 (maximum of 1.1—induced by structure and not permanent deformation). However, the stress-strain graph indicating the loading cycle of the second phase (L2) does not recover to its original position, indicating minor accumulation of damage (i.e., residual strain accumulation). In addition, on unloading, the ratio of local to global strain has a permanent average value of 1.17. Therefore, in the present study, the ratio of 1.17 is proposed to be considered as a cutoff ratio to indicate permanent damage initiation in PET-FRP laminates.

Fig. 12 presents the ratio of local to global strains plotted against the average strain for a laminate tested at room temperature. At the beginning of the curve, the ratio is close to 1, which indicates no difference in the local and global responses in the elastic phase. However, as the sample is loaded, the ratio gradually increases and then stays constant. The black dotted line in Fig. 12 illustrates the point on the curve at which the ratio of local to global strain is 1.17. After this point, in the sample, permanent damage starts accumulating.

Considering the aforementioned aspects, local and global stress-strain curves for representative samples at each tested temperature in this study were plotted. In addition, the ratios of local to global response at all temperature levels were evaluated. Considering a cutoff ratio of 1.17 to indicate damage initiation, the average strain at which the local to global ratio reaches 1.17 was recorded for all samples. Fig. 13 indicates the global and local stress-strain curves for samples tested at 25°C, 75°C, and 125°C, along with

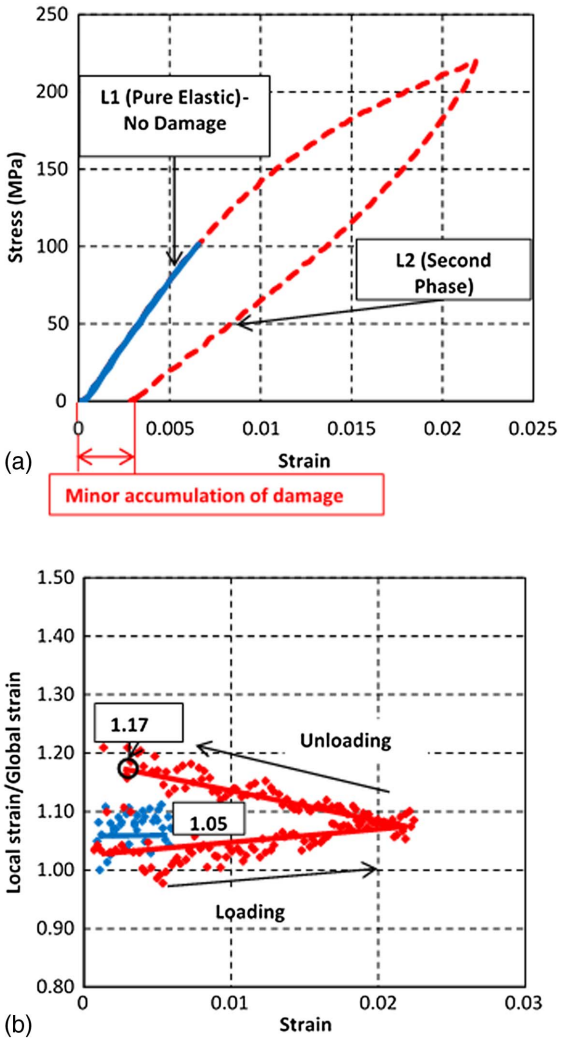

Fig. 11. Loading and unloading cycles of a PET laminate at room temperature: (a) stress-strain curves; and (b) ratio of local to global strains.

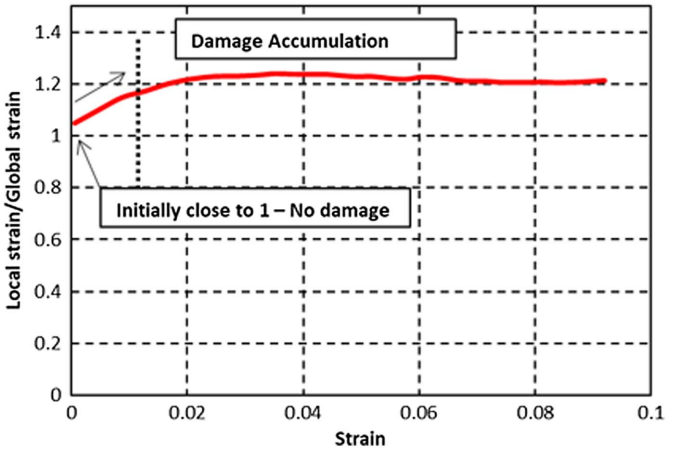

Fig. 12. Ratio of local to global strains for PET-FRP at 25°C.

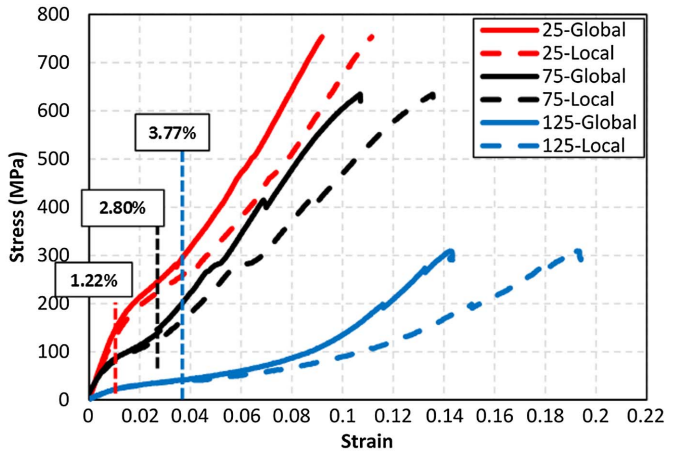

Fig. 13. Stress strain curves in terms of local and global strains for representative samples tested at 25°C, 75°C, and 125°C.

Table 6. Strain values at which damage starts to accumulate for all tested temperatures

Temperature (°C)	Strain at which damage starts to accumulate (%)
25	1.22
50	1.27
75	2.80
100	3.43
125	3.77

strain values indicating damage initiation. In addition, Table 6 presents the strain at which damage starts to accumulate for temperatures ranging from 25°C to 125°C. The values provided in Fig. 13 and Table 6 indicate an increasing trend in the strain at which damage starts accumulating with increasing temperatures. The strain at which permanent damage is initiated for samples tested at room temperature and 125°C is 1.22% and 3.77%, respectively.

Conclusion

PET-FRP laminates were tested at distinct temperatures of 25°C, 50°C, 75°C, 100°C, and 125°C to investigate the degradation of its mechanical properties at elevated temperatures. Stress-strain curves were drawn using strains obtained from DIC, and the mechanical properties, such as modulus, tensile strength, and Poisson's ratio, were discussed. The following observations and conclusions are drawn using the test results:

- PET-FRP laminates exhibit a three-stage, nonlinear stress-strain behavior. For that reason, the stress-strain curve could be divided into three stages using three moduli (E_1, E_2, and E_3) and three tensile strengths (σ_1, σ_2, and σ_3). E_1 is considered the elastic modulus, and σ_3 is the ultimate tensile strength of the laminates.
- In general, the moduli and tensile strengths of PET-FRP laminates degrade with increasing temperatures, except at 50°C, at which its tensile strength is enhanced due to curing of the epoxy; subsequently, it starts to degrade at higher temperature levels.
- PET-FRP laminates can attain high levels of ductility before failure compared with conventional FRP materials. The average value of the rupture strain is 9% for samples tested at room temperature, which increases to 14.19% at 125°C.
- The value of the Poisson's ratio of PET-FRP increases from 0.486 at room temperature to 0.573 at 125°C, indicating the so ft ening of the matrix at higher temperature levels.
- The models proposed in this study can be used by engineers as input parameters (especially in finite element modeling) when analyzing and designing externally strengthened members with PET-FRP laminates.
- Damage starts to accumulate in PET-FRP laminates at a local to global strain ratio of 1.17.
- The strains at which permanent damage is initiated increase from 1.22% at room temperature to 3.77% at 125°C.

The areas of designing and building green and circular economies that aim to develop sustainable construction materials while limiting waste of resources are of significant interest to scientists and engineers. Although not a focus in the current work, PET can be recycled to produce FRP laminates and is, thus, of interest as a potential sustainable construction material. However, the mechanical properties of such recycled material have not been evaluated and require further investigation.

Appendix: Analytical Models for the Degradation of FRP Mechanical Properties at Elevated Temperatures

Among the analytical studies, Gu and Asaro (2005) developed the following empirical model to predict the degradation of the mechanical properties of E-glass laminates at any temperature (T):

$$P(T) = P_u\left(1 - \frac{T - T_r}{T_{\text{ref}} - T_r}\right)^m \tag{7}$$

where T_{ref} = temperature at which the material property vanishes [taken as 125°C in Gu and Asaro (2005)]; T_r = room temperature; m = power law index that ranges between 0 and 1, with 0 for no degradation and 1 for linear degradation with temperature; and P_u = mechanical property at ambient temperature.

Similarly, Gibson et al. (2006) proposed a hyperbolic tangent function model to predict the mechanical properties (P) of FRPs as a function of temperature (T) using the following equation:

$$P(T) = R^n\left(\frac{P_U + P_R}{2} - \frac{P_U - P_R}{2}\tanh[k_m(T - T')]\right) \tag{8}$$

where R^n = power law factor to account for resin decomposition and is usually taken as 1; P_U = material property at room temperature; P_R = material property a ft er glass temperature and before decomposition; k_m = constant describing the extent of relaxation; and T' = mechanically determined glass transition temperature (not necessarily T_g). Both k_m and T' are determined by fitting the experimental data.

On the basis of the model proposed by Gibson et al. (2006), Yu and Kodur (2014) performed a regression analysis using experimental data on NSM CFRP rods and strips to develop constants for k_m. Eqs. (9)–(6) present the models of the elastic modulus $E(T)$ and tensile strength $f(t)$ as a function of temperature for CFRP strips and rods, respectively.

For the CFRP strip:

$$E(t) = 0.51 - 0.49\tanh[0.0035(T - 340)] \tag{9}$$

$$f(t) = 0.56 - 0.44\tanh[0.0052(T - 305)] \tag{10}$$

For the CFRP rod:

$$E(t) = 0.51 - 0.49\tanh[0.0033(T - 320)] \tag{11}$$

$$f(t) = 0.54 - 0.46\tanh[0.0064(T - 330)] \tag{12}$$

Likewise, in a more recent study, Hawileh et al. (2016) used the Gibson et al. (2006) model to propose empirical models to predict the mechanical properties of CFRP laminates, BFRP laminates, and their hybrid combination (BC) as a function of temperature. Values of k_m and T' in Eq. (8) are provided in Hawileh et al. (2016).

Bisby (2003) developed a model to evaluate the degradation of FRP mechanical properties, such as tensile modulus, strength, and bond, under elevated temperatures. The model is presented in the following equation:

$$\frac{P(T)}{P_U} = \left(\frac{1 - a}{2}\right)\tanh(-b(T - c)) + \left(\frac{1 + a}{2}\right) \tag{13}$$

where a is a constant that defines the residual value of the mechanical property; and b and c are parameters determined by a least square regression analysis using the experimental data. In his study, Bisby (2003) provided values for coefficients a, b, and c to predict the modulus and tensile strength of CFRP, GFRP, and AFRP laminates under elevated temperatures.

In another study, Wang et al. (2011) proposed the following model to describe the degradation of the tensile strength of CFRP pultruded laminates inspired by a model developed for stainless steel and cold-formed steel

$$P(T) = P_U\left[A - \frac{(T-B)^n}{C}\right] \tag{14}$$

where A, B, C, and n are temperature-dependent coefficients. The authors in Wang et al. (2011) proposed values for these parameters depending on the temperature range.

Data Availability Statement

Some or all of the data, models, or code generated or used during the study are available from the corresponding author by request (stress-strain data, Poisson's ratio data, proposed models, and damage initiation data).

Acknowledgments

The work in this paper was supported, in part, by the Open Access Program from the American University of Sharjah. This paper represents the opinions of the authors and does not mean to represent the position or opinions of the American University of Sharjah. The authors gratefully acknowledge the support of the American University of Sharjah for sponsoring this research project. The authors would also like to thank and acknowledge MAPEI for providing the epoxy, and MAEDAKOSEN for providing the PET fibers. Special thanks to Eng. Mustafa Elyoussef for his help and collaboration in conducting the experiments.

References

Al-Tamimi, A. K., R. A. Hawileh, J. A. Abdalla, H. A. Rasheed, and R. Al-Mahaidi. 2015. "Durability of the bond between CFRP plates and concrete exposed to harsh environments." *J. Mater. Civ. Eng.* 27 (9): 04014252. https://doi.org/10.1061/(ASCE)MT.1943-5533.0001226.

Ali, A., J. Abdalla, R. Hawileh, and K. Galal. 2014. "CFRP mechanical anchorage for externally strengthened RC beams under flexure." *Physics Procedia* 55: 10–16. https://doi.org/10.1016/j.phpro.2014.07.002.

Anggawidjaja, D., T. Ueda, J. Dai, and H. Nakai. 2006. "Deformation capacity of RC piers wrapped by new fiber-reinforced polymer with large fracture strain." *Cem. Concr. Compos.* 28 (10): 914–927. https://doi.org/10.1016/j.cemconcomp.2006.07.011.

ASTM. 2008. *Standard test method for tensile properties of polymer matrix composite materials*. ASTM D3039M. West Conshohocken, PA: ASTM.

Benedetti, A., P. Fernandes, J. L. Granja, J. Sena-Cruz, and M. Azenha. 2015. "Influence of temperature on the curing of an epoxy adhesive and its influence on bond behaviour of NSM-CFRP systems." *Composites Part B* 89 (Mar): 219–229. https://doi.org/10.1016/j.compositesb.2015.11.034.

Bisby, L. A. 2003. "Fire behaviour of fibre-reinforced polymer (FRP) reinforced or confined concrete." Ph.D. thesis, Dept. of Civil Engineering, Queen's Univ.

Borg, R. P., O. Baldacchino, and L. Ferrara. 2016. "Early age performance and mechanical characteristics of recycled PET fibre reinforced concrete." *Constr. Build. Mater.* 108 (Apr): 29–47. https://doi.org/10.1016/j.conbuildmat.2016.01.029.

Chowdhury, E. U., R. Eedson, L. A. Bisby, M. F. Green, and N. Benichou. 2011. "Mechanical characterization of fibre reinforced polymers materials at high temperature." *Fire Technol.* 47 (4): 1063–1080. https://doi.org/10.1007/s10694-009-0116-6.

Correia, J. R., M. M. Gomes, J. M. Pires, and F. A. Branco. 2013. "Mechanical behaviour of pultruded glass fibre reinforced polymer composites at elevated temperature: Experiments and model assessment." *Compos. Struct.* 98 (Apr): 303–313. https://doi.org/10.1016/j.compstruct.2012.10.051.

Dai, J. G., Y. L. Bai, and J. G. Teng. 2011. "Behavior and modeling of concrete confined with FRP composites of large deformability." *J. Compos. Constr.* 15 (6): 963–973. https://doi.org/10.1061/(ASCE)CC.1943-5614.0000230.

Dai, J. G., L. Lam, and T. Ueda. 2012. "Seismic retrofit of square RC columns with polyethylene terephthalate (PET) fibre reinforced polymer composites." *Constr. Build. Mater.* 27 (1): 206–217. https://doi.org/10.1016/j.conbuildmat.2011.07.058.

El-Dieb, A. S., S. Aldajah, A. Biddah, and A. Hammami. 2012. "Long-term performance of RC members externally strengthened by FRP exposed to different environments." *Arabian J. Sci. Eng.* 37 (2): 325–339. https://doi.org/10.1007/s13369-012-0177-6.

El-Hassan, H., and T. El Maaddawy. 2019. "Microstructure characteristics of GFRP reinforcing bars in harsh environment." *Adv. Mater. Sci. Eng.* 2019: 1–19. https://doi.org/10.1155/2019/8053843.

Gibson, A. G., Y. S. Wu, J. T. Evans, and A. P. Mouritz. 2006. "Laminate theory analysis of composites under load in fire." *J. Compos. Mater.* 40 (7): 639–658. https://doi.org/10.1177/0021998305055543.

Gu, P., and R. J. Asaro. 2005. "Structural buckling of polymer matrix composites due to reduced stiffness from fire damage." *Compos. Struct.* 69 (1): 65–75. https://doi.org/10.1016/j.compstruct.2004.05.016.

Hawileh, R. A., J. A. Abdalla, S. S. Hasan, M. B. Ziyada, and A. Abu-Obeidah. 2016. "Models for predicting elastic modulus and tensile strength of carbon, basalt and hybrid carbon-basalt FRP laminates at elevated temperatures." *Constr. Build. Mater.* 114 (Jul): 364–373. https://doi.org/10.1016/j.conbuildmat.2016.03.175.

Hawileh, R. A., A. Abu-Obeidah, J. A. Abdalla, and A. Al-Tamimi. 2015a. "Temperature effect on the mechanical properties of carbon, glass and carbon-glass FRP laminates." *Constr. Build. Mater.* 75 (Jan): 342–348. https://doi.org/10.1016/j.conbuildmat.2014.11.020.

Hawileh, R. A., M. Naser, W. Zaidan, and H. A. Rasheed. 2009. "Modeling of insulated CFRP-strengthened reinforced concrete T-beam exposed to fire." *Eng. Struct.* 31 (12): 3072–3079. https://doi.org/10.1016/j.engstruct.2009.08.008.

Hawileh, R. A., and M. Z. Naser. 2012. "Thermal-stress analysis of RC beams reinforced with GFRP bars." *Composites Part B* 43 (5): 2135–2142. https://doi.org/10.1016/j.compositesb.2012.03.004.

Hawileh, R. A., W. Nawaz, J. A. Abdalla, and E. I. Saqan. 2015b. "Effect of flexural CFRP sheets on shear resistance of reinforced concrete beams." *Compos. Struct.* 122 (Apr): 468–476. https://doi.org/10.1016/j.compstruct.2014.12.010.

Hawileh, R. A., H. A. Rasheed, J. A. Abdalla, and A. K. Al-Tamimi. 2014. "Behavior of reinforced concrete beams strengthened with externally bonded hybrid fiber reinforced polymer systems." *Mater. Des.* 53 (Jan): 972–982. https://doi.org/10.1016/j.matdes.2013.07.087.

Huang, L., S. S. Zhang, T. Yu, and Z. Y. Wang. 2018. "Compressive behaviour of large rupture strain FRP-confined concrete-encased steel columns." *Constr. Build. Mater.* 183 (Sep): 513–522. https://doi.org/10.1016/j.conbuildmat.2018.06.074.

Lechat, C., A. R. Bunsell, P. Davies, and B. Pet. 2011. "Tensile and creep behaviour of polyethylene terephthalate and polyethylene naphthalate fibres." *J. Mater. Sci.* 46 (2): 528–533. https://doi.org/10.1007/s10853-010-4999-x.

Ou, Y., and D. Zhu. 2015. "Tensile behavior of glass fiber reinforced composite at different strain rates and temperatures." *Constr. Build. Mater.* 96 (Oct): 648–656. https://doi.org/10.1016/j.conbuildmat.2015.08.044.

Ou, Y., D. Zhu, H. Zhang, Y. Yao, B. Mobasher, and L. Huang. 2016. "Mechanical properties and failure characteristics of CFRP under intermediate strain rates and varying temperatures." *Composites Part B* 95 (Jun): 123–136. https://doi.org/10.1016/j.compositesb.2016.03.085.

Pimanmas, A., and S. Saleem. 2018. "Dilation characteristics of PET FRP-confined concrete." *J. Compos. Constr.* 22 (3): 04018006. https://doi.org/10.1061/(ASCE)CC.1943-5614.0000841.

Reis, J. M. L., J. L. V. Coelho, A. H. Monteiro, and H. S. Da Costa Mattos. 2012. "Tensile behavior of glass/epoxy laminates at varying strain rates and temperatures." *Composites Part B* 43 (4): 2041–2046. https://doi.org/10.1016/j.compositesb.2012.02.005.

Saleem, S., Q. Hussain, and A. Pimanmas. 2017. "Compressive behavior of PET FRP-confined circular, square, and rectangular concrete columns." *J. Compos. Constr.* 21 (3): 04016097. https://doi.org/10.1061/(ASCE)CC.1943-5614.0000754.

Saleem, S., A. Pimanmas, and W. Rattanapitikon. 2018. "Lateral response of PET FRP-confined concrete." *Constr. Build. Mater.* 159 (Jan): 390–407. https://doi.org/10.1016/j.conbuildmat.2017.10.116.

Shekarchi, W. A., W. M. Ghannoum, and J. O. Jirsa. 2018. "Use of anchored carbon fiber-reinforced polymer strips for shear strengthening of large girders." *ACI Struct. J.* 115 (1): 281–291. https://doi.org/10.14359/51701092.

Wang, K., B. Young, and S. T. Smith. 2011. "Mechanical properties of pultruded carbon fibre-reinforced polymer (CFRP) plates at elevated temperatures." *Eng. Struct.* 33 (7): 2154–2161. https://doi.org/10.1016/j.engstruct.2011.03.006.

Yu, B., and V. Kodur. 2014. "Effect of temperature on strength and stiffness properties of near-surface mounted FRP reinforcement." *Composites Part B* 58 (Mar): 510–517. https://doi.org/10.1016/j.compositesb.2013.10.055.

Zhang, D., Y. Zhao, W. Jin, T. Ueda, and H. Nakai. 2017. "Shear strengthening of corroded reinforced concrete columns using pet fiber based composites." *Eng. Struct.* 153 (Dec): 757–765. https://doi.org/10.1016/j.engstruct.2017.09.030.

Zhou, F., J. Zhang, S. Song, D. Yang, and C. Wang. 2019. "Effect of temperature on material properties of carbon fiber reinforced polymer (CFRP) tendons: Experiments and model assessment." *Materials* 12 (7): 1025. https://doi.org/10.3390/ma12071025.